
CLINICAL GRADING OF ORAL MUCOSA BY CURVE-FITTING OF CORRECTED AUTOFLUORESCENCE USING DIFFUSE REFLECTANCE SPECTRA

Rupananda Jayachandra Mallia, PhD,¹ Narayanan Subhash, PhD,¹ Anitha Mathews, MD,² Rejnish Kumar, MD,³ Shiny Sara Thomas, MSc,¹ Paul Sebastian, MS,⁴ Jayaprakash Madhavan, MD⁵

¹ Biophotonics Laboratory, Centre for Earth Science Studies, Trivandrum, India. E-mail: subhashn@cessind.org

² Department of Cytopathology, Regional Cancer Centre, Trivandrum, India

³ Department of Radiation Oncology, Regional Cancer Centre, Trivandrum, India

⁴ Division of Surgical Oncology, Regional Cancer Centre, Trivandrum, India

⁵ Department of Radiotherapy, Regional Cancer Centre, Trivandrum, India

Accepted 24 July 2009

Published online 13 October 2009 in Wiley InterScience (www.interscience.wiley.com). DOI: 10.1002/hed.21251

Abstract: *Background.* Laser-induced autofluorescence (LIAF) and diffuse reflectance (DR) were collectively used in this clinical study to improve early oral cancer diagnosis and tissue grading.

Methods. LIAF and DR emission from oral mucosa were recorded on a fiber-optic spectrometer by illumination with a 404-nm diode laser and tungsten halogen lamp in 36 healthy volunteers and 40 lesions of 20 patients.

Results. Absorption dips in LIAF spectra at 545 and 575 nm resulting from changes in oxygenated hemoglobin were corrected using DR spectra of the same site. These corrected spectra were curve-fitted using Gaussian spectral functions to determine constituent emission peaks and their relative contribution. The Gaussian peak intensity and area ratios F500/F635 and F500/F685 were found to be useful indicators of tissue transformation. The diagnostic capability of various ratios in differentiating healthy, hyperplastic, dysplastic, and squamous

cell carcinomas (SCCs) were examined using discrimination scatterplots.

Conclusions. The LIAF/DR technique, in conjunction with curve-fitting, differentiates different grades of dysplasia and SCC in this clinical trial and proves its potential for early detection of oral cavity cancer and tissue grading. © 2009 Wiley Periodicals, Inc. *Head Neck* 32: 763–779, 2010

Keywords: oral squamous cell carcinoma; oral dysplasia; optical diagnosis; oxygenated hemoglobin absorption; curve-fitted Gaussian spectral functions

Oral cancer is an imperative and growing public health concern around the world because of its prevalence. Nearly 85% of malignancies affecting the oral cavity are squamous cell carcinoma (SCC) arising from the epithelial tissues.¹ Oral SCC has been associated with a well-defined group of risk factors. Dysplasias are pre-invasive neoplastic lesions that are seen in the oral cavity as erythroplakia and leukoplakia, with their chances of conversion to SCC being roughly 90% and 10%, respectively.² Early

Correspondence to: N. Subhash

Contract grant sponsor: Department of Science and Technology, Government of India; contract grant sponsor: Center for Earth Science Studies; contract grant number: Plan-223 project.

© 2009 Wiley Periodicals, Inc.

detection of neoplastic changes in the oral cavity is the best method to improve the quality of life of patients because, at these embryonic stages, their eradication/treatment/management measures would be immense and more effective. To ensure accurate histopathologic diagnosis the biopsy site must be selected precisely; an appropriate biopsy would include tissue from the worst part of the lesion. However, in usual practice, even for the experienced clinicians, it is not easy to distinguish visually between benign and malignant/premalignant area within a suspicious lesion because the severity of the lesion varies from 1 portion to another. Thus, a non-representative tissue sampling could lead to repeated biopsies to the discomfort of patients. Again, it is difficult to visually identify the microscopic epithelial alterations, and often, oral mucosa with inflammation or irritation could resemble premalignant conditions, making visual identification subjective and the ensuing biopsy-guided histopathology more challenging and time consuming.

In this context, a noninvasive procedure that can identify and classify oral lesions in their early stage has great significance because it will enable optimum patient care and improve survival rates. In recent years, various optical spectroscopy techniques have been gaining greater acceptance because of improvements in detection sensitivities, and because of the noninvasive nature of tissue characterization they are termed "optical biopsies." Among these techniques, the potentials of laser-induced autofluorescence (LIAF) and tissue reflectance are immense, yet nevertheless they have not reached the acceptance levels for use in a clinical environment for detection and grading of malignant and premalignant superficial tumors or lesions.

Autofluorescence arises as a result of emission from various fluorophores, such as elastin, collagen, nicotinamide adenine dinucleotide hydrogenase (NADH), and flavin adenine dinucleotide (FAD) present in human tissue.^{3,4} During the process of carcinogenesis, morphohistologic characteristics and physiochemical compositions of these fluorophores undergo modification from normal levels, making LIAF spectral features sensitive to tissue alterations. Many researchers have successfully used the potential of LIAF spectroscopy for noninvasive investigation of malignant lesions under *in vivo* conditions.⁵⁻¹⁰

The autofluorescence spectra of oral mucosa were studied in detail by Ingrams et al¹¹ and

optimal excitation wavelengths were identified by Heintzelman et al¹² for *in vivo* fluorescence detection of oral neoplasia. Noninvasive diagnosis of oral cancer based on native tissue autofluorescence was also carried out by Gillenwater et al¹³ with good sensitivity and specificity. Savage et al¹⁴ used different intensity ratios, including the red/blue ratios at various excitation wavelengths to differentiate malignant and normal lateral tongue. An *ex vivo* study conducted by Roy et al¹⁵ clearly depicted consistent spectral differences when dysplastic and cancerous tissues were compared with normal tissue.

Fluorescence imaging systems were used by many researchers to facilitate screening of the whole lesion area. Scott et al¹⁶ used red to green fluorescence image intensity ratios, which showed good enhancement in contrast between control and cancerous lesions, on topical application of 5-aminolevulinic acid (5-ALA). By using red-to-blue fluorescence image intensity ratios in a diagnostic algorithm, Zheng et al¹⁷ discriminated and classified normal, carcinoma *in situ* (CIS), and invasive SCC with high specificity and sensitivity.

Svistun et al¹⁸ recorded fluorescence emission from freshly resected oral lesions on a Canon camera (Canon, Tokyo, Japan), with 100-mm microlens and broad-band (60-nm) filter, and obtained a sensitivity of 91% and specificity of 86% to discriminate normal tissue from neoplasia, which compares favorably with the white-light sensitivity of 75% and specificity of 43%. Very recently, Lane and colleagues¹⁹ developed a simple and cost-effective handheld device that allows the clinician to discriminate malignant tissues by direct visualization of tissue fluorescence. Clinical trials with this system on 44 patients gave a sensitivity of 98% and a specificity of 100% in discriminating normal mucosa from abnormal severe dysplasia CIS and invasive carcinoma.

De Veld et al²⁰ used statistical methods such as principal component analysis (PCA) and applied artificial neural networks and receiver operating characteristic (ROC) curves for comparison of autofluorescence and diffuse reflectance (DR) methods in distinguishing premalignant lesions from normal/benign mucosa. In another study, they used autofluorescence and DR spectroscopy separately and in combination for oral cancer diagnosis and found that autofluorescence corrected for blood absorption using DR improves the classification of

cancer.²¹ Recently, by using trimodel spectroscopy, which is a combination of autofluorescence, DR, and light-scattering spectroscopy, Muller et al²² achieved a specificity and sensitivity of 96%. In an ex vivo study, Subhash et al²³ found that the DR ratio (R540/R575) of the oxygenated hemoglobin absorption dips at 540 and 575 nm can be used to distinguish different grades of oral cavity SCC, which was later confirmed and used to detect early stages of cancer in a clinical trial by Mallia et al.²⁴

In this clinical study, LIAF spectra corrected for blood absorption were analyzed by curve-fitting and scatterplots of the ratios of the deconvoluted Gaussian peak amplitude; the area of constituent bands at 500, 635, and 685 nm were used to differentiate various tissue types, such as normal, hyperplastic/hyperkeratotic (benign), intra-premalignant dysplasias (mild, moderate, and severe), and different stages of SCC (well-differentiated, moderately differentiated, and poorly differentiated). The results of a comparative evaluation of the curve-fitted ratios with those derived from raw LIAF spectral data are also presented. This study has designed an optical modality that could be a noninvasive alternate to histopathology by providing total tissue grading—or at least as an adjunct—to the clinicians to locate the most abnormal portion of lesion under question for biopsy that could eliminate the subjective nature of histopathology because of its dependence on subjective clinically guided biopsy.

MATERIALS AND METHODS

Instrumentation. The laser-induced fluorescence and reflectance spectroscopy (LIFRS) system (see Figure 1), consisting of a diode laser (Model: 404 nm, 50 mW, CW; StockerYale Inc, Dollard-des-Ormeaux, QC, Canada) and a tungsten halogen lamp (Model LS-1; Ocean Optics, Dunedin, FL) that could be switched for sequential recording of LIAF and DR spectra of tissues. A bifurcated optical fiber guides the light output to the oral tissue through a 15-cm-long, 6-mm-diameter stainless steel probe that has a central fiber to deliver the excitation beam and 6 surrounding fibers (each of 400- μ m diameter) to collect the LIAF/DR emission. The light emanating from the sample is delivered to a miniature fiber-optic spectrometer (Model USB 2000FL

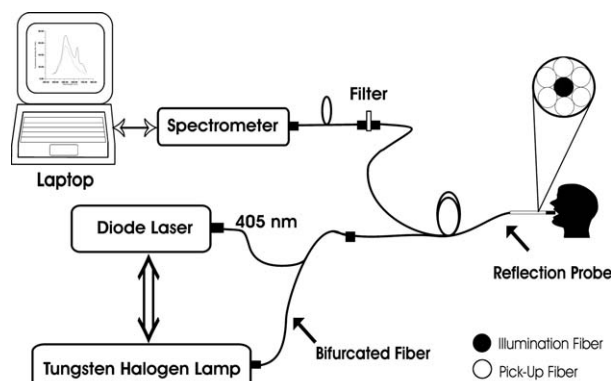


FIGURE 1. Schematic of LIFRS system for LIAF and DR measurements. LIFRS, laser-induced fluorescence and reflectance spectroscopy; LIAF, laser-induced autofluorescence; DR, diffuse reflectance.

VIS-NIR; Ocean Optics) connected to the USB port of a laptop computer. During fluorescence studies, a long-wavelength pass filter (GG420; Schott Glass Technologies, Hughesstown, PA) was used to block the back-scattered laser light from entering the spectrometer. Technical details of the experimental system are given elsewhere.^{24,25}

Data Acquisition and Preprocessing. The laser beam was focused onto the fiber tip so that the laser output (1 mW) at the probe tip has a Gaussian intensity profile. The OOI Base32 software (Ocean Optics) was configured to record the spectra, averaged for 40 scans, with a box-car width of 10 nm and an integration time of 100 ms, and the LIAF and DR spectra were acquired with a spectral resolution of 10 nm.

Before LIAF and DR measurements from the lesion, the background spectrum was recorded and the OOI Base32 software was configured to automatically subtract the same during each measurement. Considering the heterogeneous nature of oral cavity lesions, 15 sets of LIAF and DR spectral measurements were taken from each site in the 420- to 720-nm spectral range, and the mean value was used in data analysis.

Study Protocol and Clinical Measurements. The clinical study included 36 healthy volunteers, with no clinically observable lesions or inflammatory conditions in their oral cavity, and 20 patients, with measurements taken from 40 sites, having clinically low/high-risk lesions in their oral cavity. These 40 sites included

pathologically confirmed hyperplastic ($n = 8$), mild dysplastic ($n = 5$), moderately dysplastic ($n = 7$), severely dysplastic ($n = 5$), well-differentiated SCC ($n = 4$), moderately differentiated SCC ($n = 5$), and poorly differentiated SCC ($n = 6$) lesions. In each patient, an experienced head and neck clinician selected the suspicious lesions for spectral studies and recorded the visual imprint. Spectral measurements were carried out at the outpatient clinic of the Regional Cancer Centre (RCC), Trivandrum, India. Prior approval for the clinical trial and the study protocol was obtained from the Ethics Committee of RCC. After explaining the modalities of the study, written informed consent was obtained from each patient/volunteer before enrollment.

As a first step, the patients/volunteers were directed to hold 0.9% saline solution in their mouth for 2 to 3 minutes to reduce the effects of recently consumed food. The control LIAF and DR spectra were measured from the oral cavity of healthy volunteers at 13 different anatomic locations: the right and left buccal mucosa, the gingiva, the upper and lower alveolus, the floor of mouth, the hard and soft palate, the dorsal tongue, the lateral border tongue, the ventral tongue, the inner lip, the vermilion border of lip, and the transition to floor of mouth. A pictorial representation of different anatomic sites within the human oral cavity is given elsewhere.²⁵ In healthy volunteers, strong emissions were observed at 635, 685, and 705 nm from the dorsal and the lateral sides of tongue and the vermilion border of the lip, as in cancerous lesions. Therefore, these sites were excluded from the present study.²⁵

After completion of in vivo LIAF and DR measurements in patients, incision biopsies were taken from the measurement sites, fixed in 10% normal formalin, and sent for histopathologic analysis. Histology slides were prepared from the biopsies and classified by an experienced pathologist blinded to the fluorescence spectral results. To avoid intraobserver variability, an experienced pathologist at the RCC graded all histology slides at the same time. In the case of healthy volunteers, visual inspection was carried out instead of biopsy. After classification, spectroscopic data were correlated with the histopathologic findings. An independent Student's t test was performed on the fluorescence ratios F500/F635 and F500/F685, to assess their statistical significance in discerning different tissue types.

Data Processing. Artifacts attributed to oxygenated hemoglobin absorption were noticed in the LIAF spectra at 545 and 575 nm.²⁵ Various refining models have been used by different groups to correct these absorption dips and recover intrinsic autofluorescence spectra from the recorded fluorescence spectra.^{26,27} However, we used a first-order approximation that involves division of LIAF with the DR spectra from the same tissue site, to remove the absorption artifacts, as given by De Veld et al²¹:

$$F_i(\lambda) = Fr(\lambda)/R_d(\lambda)^{x(\lambda)} \quad (1)$$

where $F_i(\lambda)$ is the corrected autofluorescence from the fluorophores, $Fr(\lambda)$ is the recorded autofluorescence, $R_d(\lambda)$ is total diffuse reflectance, and $x(\lambda)$ is a variable power, depending on the tissue under investigation. In an early study, we observed that the HbO₂ absorption artifacts depend on the lesion type, showing marked variations at sites such as the tongue, gingiva, alveolus, and buccal mucosa.²⁵ Thus, various values between 0.20 and 0.45 were chosen for the variable power x to smooth out the absorption dips. It was noticed that while applying this correction, the overall fluorescence intensity is reduced by nearly 50% for $x = 0.25$. Figures 2A and 2B represent the in vivo LIAF spectra and the derived corrected fluorescence spectra of normal and malignant buccal mucosa for $x = 0.20$.

Curve-fitting. The mean corrected LIAF spectra from healthy mucosa and various grades of malignant lesions were analyzed using a curve-fitting program (Origin, version 6.0, MicroCal LLC/GE Healthcare, Piscataway, NJ) with Gaussian spectral functions, to precisely determine the peak position, intensity, and bandwidth (full width at half-maximum [FWHM]) of the constituent bands in the spectra during tissue transformation. The fitting program uses the Marquardt–Levenberg algorithm that finds the true absolute minimum value of the sum of squared deviations (the value of chi-square) by an iterative process. The quality of fitting is determined by the random spread in residuals of fitting, correlation coefficient r^2 (close to unity), and low chi-square values.²⁸ Fluorescence ratios that relate to tissue transformations were determined from the Gaussian peak

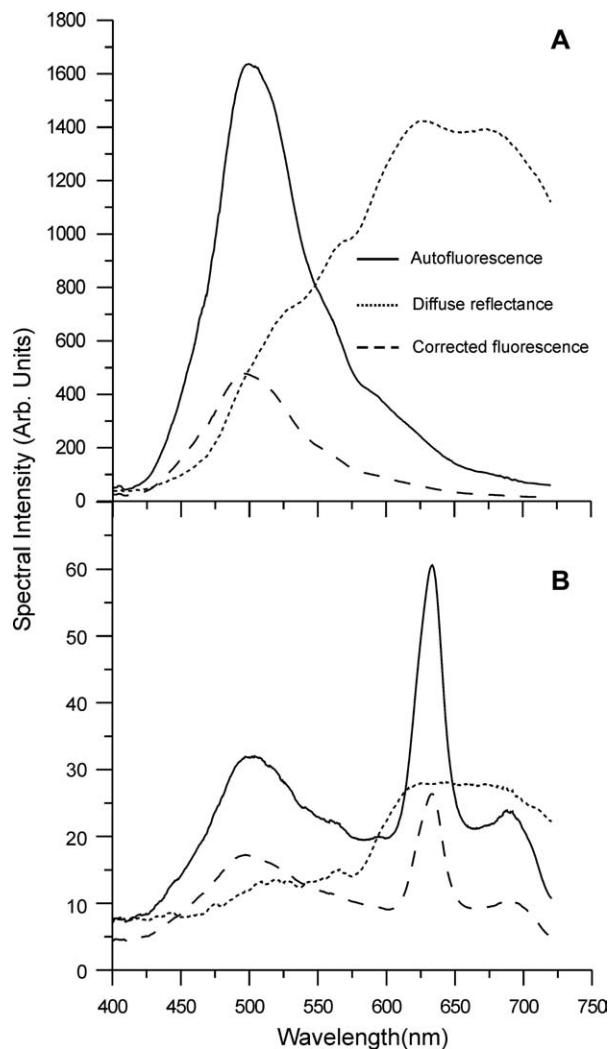


FIGURE 2. Average in vivo autofluorescence and DR spectra from healthy buccal mucosa (**A**) and well-differentiated SCC buccal lesion of a patient (**B**), and the corresponding corrected fluorescence spectra for $x = 0.2$. DR, diffuse reflectance; SCC, squamous cell carcinoma.

amplitude and curve area of the constituent bands deconvoluted by curve-fitting.

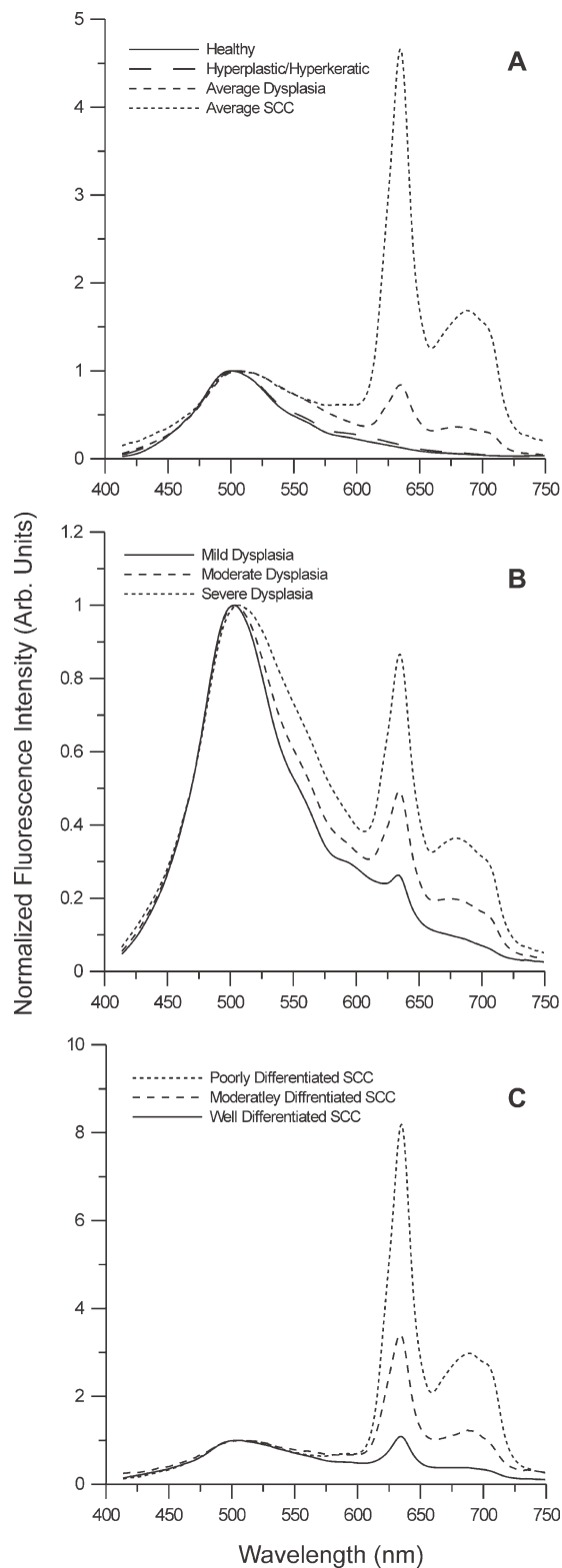
RESULTS

LIAF Spectral Features. The in vivo fluorescence measurements were carried out from apparently normal, malignant, and suspicious margin areas of oral lesions. We have grouped the oral mucosa into 4 major categories based on histopathologic results. The first and second groups consisted of normal and hyperplastic/hyperkeratotic mucosa, whereas the third and fourth

groups consisted of premalignant dysplastic tissues and malignant SCC lesions. The SCC group was further divided into 3 intra-groups consisting of well-differentiated SCC, moderately differentiated SCC, and poorly differentiated SCC, with increasing grades of malignancy. Similarly, premalignant dysplasias were classified into 3 intra-grades: mild, moderate, and severe. Histopathologic analysis of biopsy samples in a previous study showed that oral mucosa adjoining malignant sites in patients are not usually normal, but display various degrees of epithelial dysplasia and hyperplasia.²⁵ Therefore, instead of using LIAF data from apparently normal lesions of patients as control, we used the mean LIAF spectral data values of the oral mucosa recorded from 36 healthy volunteers as control in this study.

The LIAF spectra show a broad autofluorescence peak at 500 nm that is characteristic of epithelial tissues. Compared with the 500-nm autofluorescence emission from normal tissues, abnormal tissues exhibit lower fluorescence intensities that decreased with increasing grades of abnormality. In SCC and dysplastic tissues the autofluorescence peak appears broadened and red-shifted by about 20 nm. The abnormal tissues have 2 additional peaks centered about 635 and 685 nm, whereas a broad peak with a shoulder around 700 nm is observed in SCC lesions resulting from the porphyrin emission. Figure 3A represents the mean in vivo LIAF spectra of the 4 major categories studied, ie, the healthy/normal, benign hyperplastic/hyperkeratotic, premalignant dysplastic, and cancerous oral SCC mucosa, after normalization to the intensity of the autofluorescence peak at 500 nm. In lesions pathologically diagnosed as SCC, the peak at 635 nm is very prominent, compared with dysplastic tissues, and an additional peak around 685 nm is observed, with the 705-nm peak appearing as a shoulder. Nevertheless, the 705-nm peak is less prominent in dysplastic tissues and the 685-nm peak appears broadened. In hyperplastic tissues the 705-nm peak is absent and the intensity of the 635-nm peak is very small, whereas in healthy mucosa these 3 peaks are absent. Absorption anomalies arising from the presence of HbO₂, which appear as dips at 545 and 575 nm in the LIAF in the entire range of normal and abnormal tissues, were corrected using equation (1), with the help of the mean site-specific DR spectra recorded from healthy volunteers.

Figures 3B and 3C compare the corresponding spectral intensity variations of intra-dysplastic and SCC lesions. It is seen that the



fluorescence intensity at 635 and 685 nm increases with the inter-/intra-grade of tissue abnormality, and serves as a first-hand indicator of the grade of cancer. Corresponding increases in normalized fluorescence intensities at 635 and 685 nm for different tissue types—healthy, hyperplastic/hyperkeratotic, dysplastic, SCC and intra grades of dysplasia, and SCC—are plotted in Figures 4A to 4C.

Curve-fit Analysis. The corrected LIAF spectra from normal oral mucosa of healthy volunteers, and abnormal mucosa of patients obtained during the clinical trials, were analyzed by curve-fitting. It was observed that 2 Gaussian peaks were sufficient to fit the normal and hyperplastic/hyperkeratotic tissue spectrum with good values of the correlation coefficient r^2 and chi-square, whereas 4 peaks were required to fit various grades of dysplastic tissue spectra. Conversely, 4 to 5 peaks were required to obtain optimal values of r^2 and chi-square for intra-malignant tissues. Table 1 shows the peaks center, amplitude, width (FWHM), and Gaussian curve area of the deconvoluted peaks in the corrected LIAF spectra, along with the r^2 and chi-square values of fitting for the different types of tissues measured in vivo.

Figures 5A and 5B show the curve-fitted mean LIAF spectrum of normal buccal mucosa and moderately differentiated SCC lesions, with their deconvoluted constituent bands. As can be seen from Figures 5A and 5B, the best fit of the corrected autofluorescence spectra of healthy population was achieved with peaks at 500.7 and 549 nm, whereas mild dysplasia spectra were fitted with peaks at 506.6, 586, 633, and 683 nm and severe dysplasia with peaks at 508, 589, 634, and 683 nm. In the SCC domain, well-

FIGURE 3. Average in vivo LIAF spectra from oral mucosa normalized to the intensity at 500 nm for normal/healthy, hyperplastic/hyperkeratotic, average dysplastic, average SCC (A); intra grades of dysplastic lesions (mild, moderate, and severe) (B); and intra-grades of SCC (well-differentiated, moderately differentiated, poorly differentiated) (C). The normal spectrum represents the average of 10 spectral measurements from 11 anatomic sites of the oral cavity in 36 healthy volunteers, whereas the hyperplastic spectra represent the average of 10 spectral measurements from 8 lesions. Mild, moderate, and severe dysplastic spectra represent the average of 10 spectral measurements each in 5, 7, and 5 lesions, respectively. Well-differentiated, moderately differentiated, and poorly differentiated SCC spectra represent the average of 10 spectral measurements each in 4, 5 and 6 lesions, respectively. LIAF, laser-induced autofluorescence; SCC, squamous cell carcinoma.

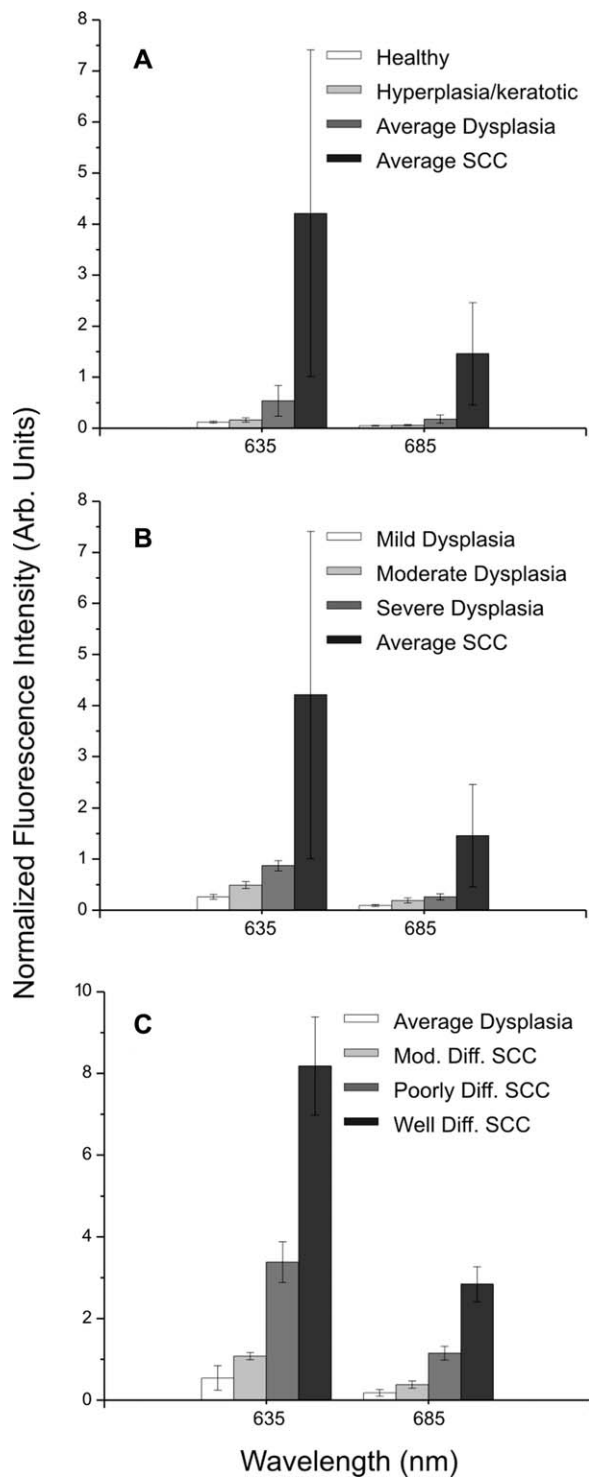


FIGURE 4. Comparison of peak intensities at 635 and 685 nm in the 500-nm-normalized LIAF spectra for normal, hyperplastic/hyperkeratotic, average dysplasia, average SCC (A); intra grades of dysplasia and average SCC (B); and intra grades of oral SCC and average dysplasia in vivo, with their SDs (C). LIAF, laser-induced autofluorescence; SCC, squamous cell carcinoma.

differentiated SCC and moderately differentiated SCC spectra required 4 peaks, whereas an additional peak at 705 nm was essential in the case of poorly differentiated SCC lesions for a good fit (Table 1).

As the tissue abnormality increased, a red-shift was observed for the 2 deconvoluted peaks of normal mucosa. In the case of the 500.7-nm peak, the red-shifts were 6.6, 8.0, 8.1, 8.8, 9, and 10.1 nm, respectively, for mild dysplasia, moderate dysplasia, severe dysplasia, well-differentiated SCC, moderately differentiated SCC, and poorly differentiated SCC lesions, whereas the corresponding shifts at 549 nm were 37.0, 38.3, 40.1, 40.5, 50.6, and 71.0 nm, respectively. In addition, the Gaussian curve area under different peaks showed substantial variation with increasing grades of tissue abnormality. For example, the Gaussian curve area and amplitude of 500.7- and 549-nm peaks showed a decreasing trend with tissue abnormality (Table 1). The curve area of the 500.7- and 549-nm peaks decreased by 39% and 14%, respectively, during tissue transformation from normal to hyperplastic, whereas for transformation from hyperplastic to premalignant mild dysplastic tissues the decrease was of the order of 26% and 36%, respectively. Gaussian area and amplitude of these peaks also showed a decreasing trend with increasing grade, within different grades of dysplasia and SCC.

For the 633.7- and 682.7-nm peaks seen in intra-grades of dysplasia and SCC, the curve-fitted area and amplitude values showed an increasing trend with increase in malignancy. During tissue transformation from mild dysplasia to the severe grade of dysplasia, the increases in the 633.5-nm area and amplitude were 100% and 131%, respectively, whereas the corresponding enhancements at 680.8 nm were 101% and 29%, respectively. During tissue transformation from severe dysplasia to well-differentiated SCC, the increases in the area and amplitude at 633.8 nm were 19% and 63%, whereas the corresponding enhancements at 682.5 nm were 25% and 8%, respectively.

Corrected and Curve-fitted LIAF Ratios. Table 2 shows the inter-variations of fluorescence ratios, F_{500}/F_{635} and F_{500}/F_{685} , of the most prominent peaks derived from the curve-fitted amplitude, area, and corrected spectral intensities and the variation with respect to different grades of abnormal lesions under in vivo

Table 1. Gaussian curve-fitted parameters of the mean corrected in vivo LIAF spectra for different tissue types.

Tissue type	Peak center, nm	FWHM, nm	Gaussian area	Gaussian amplitude	r^2	Chi-square value
Normal ($n = 36$)	500.7 \pm 0.6	55.5 \pm 1.2	33,583 \pm 3248	482.0 \pm 24.0	.99	9.5
	549.0 \pm 0.5	131.1 \pm 0.5	32,991 \pm 2234	200.0 \pm 16.0		
Hyperplasia ($n = 8$)	501.0 \pm 0.2	53.7 \pm 3.2	20,455 \pm 3872	305.0 \pm 32.0	.99	13.9
	549.0 \pm 0.5	129.6 \pm 2.3	28,408 \pm 1923	163.0 \pm 17.0		
	506.6 \pm 0.5	65.7 \pm 0.5	16,239 \pm 1756	82.0 \pm 16.0		
Mild dysplasia ($n = 5$)	586.0 \pm 0.9	153.2 \pm 0.9	18,234 \pm 2345	129.7 \pm 17.0	.99	21.1
	633.5 \pm 0.2	20.9 \pm 0.4	865 \pm 154	15.3 \pm 2.8		
	680.8 \pm 0.7	59.9 \pm 1.1	776 \pm 134	12.7 \pm 1.4		
Moderate dysplasia ($n = 7$)	508.0 \pm 0.6	65.3 \pm 2.4	10,583 \pm 1945	80.0 \pm 34.0	.99	17.1
	587.3 \pm 0.4	164.7 \pm 3.5	12,991 \pm 2784	122.0 \pm 14.0		
	633.7 \pm 0.1	21.1 \pm 0.4	1222 \pm 236	26.2 \pm 4.7		
	682.7 \pm 0.2	55.0 \pm 2.1	1185 \pm 156	15.8 \pm 1.2		
Severe dysplasia ($n = 5$)	508.1 \pm 0.7	68.7 \pm 0.7	7200 \pm 450	64.0 \pm 23.0	.99	16.2
	589.1 \pm 0.3	169.2 \pm 2.5	6991 \pm 510	86.5 \pm 9.0		
	633.8 \pm 0.1	20.2 \pm 0.1	1734 \pm 239	35.4 \pm 3.7		
	682.5 \pm 0.6	57.1 \pm 0.8	1567 \pm 198	16.3 \pm 2.2		
Well-differentiated SCC ($n = 4$)	508.8 \pm 0.3	72.5 \pm 0.5	6042 \pm 1278	27.1 \pm 3.5	.99	20.5
	589.5 \pm 0.4	181.8 \pm 1.2	2779 \pm 124	66.1 \pm 7.5		
	634.3 \pm 0.1	17.0 \pm 3.3	2065 \pm 237	51.6 \pm 6.4		
	685.3 \pm 1.0	43.7 \pm 0.2	1961 \pm 218	17.6 \pm 1.2		
Moderately differentiated SCC ($n = 5$)	509.0 \pm 1.2	72.3 \pm 0.1	2071 \pm 105	15.5 \pm 1.7	.99	21.4
	599.6 \pm 4.3	178.9 \pm 3.4	2893 \pm 145	19.4 \pm 2.3		
	634.8 \pm 0.6	19.1 \pm 1.3	3099 \pm 164	87.6 \pm 6.5		
	685.8 \pm 1.4	41.6 \pm 0.5	2393 \pm 191	26.7 \pm 4.5		
Poorly differentiated SCC ($n = 6$)	510.1 \pm 1.2	73.7 \pm 0.3	1132 \pm 55	14.0 \pm 1.8	.99	31.4
	621.3 \pm 5.2	194.1 \pm 3.6	2654 \pm 83	298.0 \pm 34.0		
	634.9 \pm 1.1	19.1 \pm 1.5	4559 \pm 542	1898.0 \pm 233.0		
	685.3 \pm 1.3	36.6 \pm 1.7	3100 \pm 135	682.0 \pm 49.0		
	705.2 \pm 2.3	17.4 \pm 2.4	964 \pm 105	451.0 \pm 33.0		

Abbreviations: LIAF, laser-induced autofluorescence; FWHM, full width at half-maximum; r^2 , correlation coefficient; SCC, squamous cell carcinoma. Note: The numbers of different mucosa types are represented in parentheses.

conditions. It can be seen that ratios determined from corrected autofluorescence showed enhanced variation with tissue abnormality. A deviation of 77% and 72% was observed respectively in the fluorescence intensity ratios, F500/F635 and F500/F685, computed from corrected LIAF spectra as malignancy changed from well-differentiated SCC to poorly differentiated SCC, whereas the corresponding Gaussian curve area ratios had a variation of 90% and 85%, respectively. Further, the Gaussian amplitude ratio F500/F635 was found to dramatically decrease by 90% from 0.72 to 0.07 and the F500/F685 ratio by 88%, from 1.95 to 0.23, as tissue transformed from well-differentiated SCC to poorly differentiated SCC. Delineation within dysplastic lesions was possible with better contrast for the Gaussian curve area and amplitude ratios than corrected raw spectral ratios during tissue proliferation from mild to moderate and moderate to severe dysplasia. During transformation

from dysplasia to SCC, the averaged F500/F635 and F500/F685 ratio values for different grades of dysplasia and SCC derived from corrected LIAF spectra showed a variation of 77% and 61%, respectively, whereas the corresponding Gaussian curve area ratios showed a variation of 88%. Further, the Gaussian amplitude ratio F500/F635 was found to significantly decrease by 89%, from 3.23 to 0.34, and the F500/F685 ratio by 82%, from 5.14 to 0.93, during transformation from dysplasia to SCC.

DISCUSSION

LIAF Spectral Features. The broad autofluorescence emission at about 500 nm, also known as the blue peak, was assigned to the endogenous fluorophores such as NADH, FAD, collagen, elastin, and amino acids.^{3,4,30} As reported

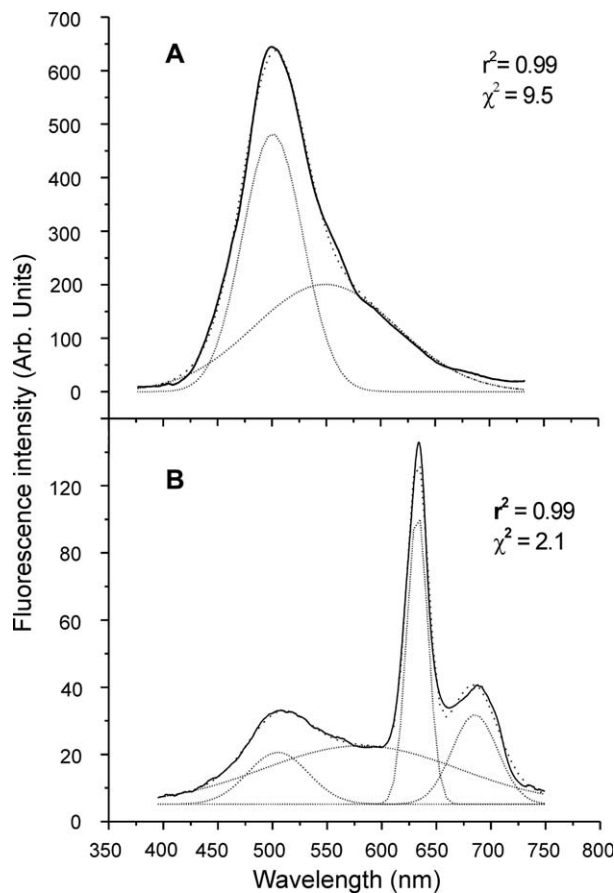


FIGURE 5. Results of curve-fitting of the corrected mean LIAF spectrum of buccal mucosa showing constituent bands from 36 healthy volunteers (A) and 5 moderately differentiated SCC lesions (B). Dots on the LIAF spectrum are the data points; the solid line is the curve-fitted line, and the dotted lines represent the constituent bands derived by curve-fitting. LIAF, laser-induced autofluorescence; SCC, squamous cell carcinoma.

earlier,^{4,31,32} the intensity of the blue peak is lower in malignant lesions compared with that in normal. We have noticed that the intensity of this peak decreases with increasing grades of abnormality. In contrast, the LIAF intensities in the red spectral region (600–710 nm) were found to increase for abnormal tissues compared with those in normal tissues (Figure 3A). In malignant and dysplastic tissues, besides the PpIX emission peak at 635 nm,^{32,33,34} we have noticed a new peak at 685 nm. Further, the 705-nm peak is not prominent for all grades of malignancy, but its contribution in the overall LIAF spectra helps in broadening the 685-nm peak (Figures 3B and 3C).

We have noticed that the 685-nm peak, which is very prominent in SCC, is absent in healthy volunteer tissues and in the

Table 2. Mean LIAF spectral ratios derived from Gaussian curve area, amplitude, and raw spectral intensities under in vivo environment for different tissue types.

Tissue type (#)	F500/F635		F500/F685	
	Raw	G area	Raw	G area
Mild dysplasia (5)	4.20 ± 0.55	18.77 ± 1.23	5.20 ± 0.45	20.92 ± 1.80
Moderate dysplasia (7)	2.50 ± 0.67 (40)	8.34 ± 1.46 (56)	3.80 ± 0.57 (27)	8.39 ± 2.23 (60)
Severe dysplasia (5)	1.40 ± 0.31 (24)	5.15 ± 0.86 (50)	3.32 ± 0.56 (13)	4.60 ± 0.67 (45)
Average dysplasia (15)	2.70 ± 0.51	10.42 ± 1.20	4.10 ± 0.32	11.30 ± 1.56
WDSCC (4)	1.20 ± 0.55 (14)	2.85 ± 0.36 (45)	2.65 ± 0.45 (20)	2.68 ± 0.26 (41)
MDSCC (5)	0.40 ± 0.55 (67)	0.83 ± 0.20 (71)	1.39 ± 0.26 (48)	1.21 ± 0.38 (55)
PDSCC (6)	0.24 ± 0.55 (50)	0.30 ± 0.02 (64)	0.75 ± 0.27 (46)	0.40 ± 0.31 (67)
Average SCC (15)	0.61 ± 0.55 (77)	1.32 ± 0.25 (88)	1.60 ± 0.33 (61)	1.43 ± 0.32 (88)
			G amplitude	G amplitude
			4.80 ± 0.55	6.85 ± 0.88
			3.80 ± 1.09 (36)	5.06 ± 0.66 (27)
			1.85 ± 0.55 (34)	3.92 ± 0.52 (23)
			3.23 ± 0.73	5.14 ± 0.69
			0.72 ± 0.11 (61)	1.95 ± 0.20 (50)
			0.24 ± 0.09 (67)	0.61 ± 0.22 (69)
			0.07 ± 0.02 (85)	0.23 ± 0.12 (63)
			0.34 ± 0.01 (89)	0.93 ± 0.18 (82)

Abbreviations: LIAF, laser-induced autofluorescence; G, Gaussian; WDSCC, well-differentiated squamous cell carcinoma; MDSCC, moderately differentiated squamous cell carcinoma; PDSCC, poorly differentiated squamous cell carcinoma.

Note: In the first column, the numbers (#) of tissues studied are represented in parentheses. Elsewhere, variation from the lower grade is shown in parentheses.

contralateral mucosa of patients and, thus, cannot be attributed to chlorophyll fluorescence from leafy vegetables or recently consumed food, as proposed earlier.²⁰ High-performance liquid chromatograms of tumor and normal colorectal tissues have shown the presence of a higher concentration of coproporphyrin III, which is a precursor of PpIX in the heme synthesis, in malignant tissues.³⁵ In the same study, peaks at 635 and 685 nm were observed when coproporphyrin III dissolved in methanol was excited with 505-nm light. Nevertheless, there is a possibility for accumulation of endogenous fluorophore coproporphyrin III when the protoporphyrin IX activity is reduced, especially in SCC and dysplastic tissues, resulting in a strong fluorescence at 685 nm. However, the contribution of the 705-nm peak is substantial, particularly in poorly differentiated SCC lesions, whereas in other malignant and dysplastic lesions a broadening of only the 685-nm peak is seen, showing higher garnering of PpIX in poorly differentiated SCC lesions.

Figures 4A to 4C depict the variation in normalized fluorescence intensities at 635 and 685 nm within the diversified tissue types. With respect to the fluorescence intensity changes, the average intensity at 635 and 685 nm for dysplastic lesions shows an increase of about 2-fold with respect to well-differentiated SCC lesions, whereas the variation is about 3-fold for moderately differentiated SCC lesions. Poorly differentiated SCC lesions show the maximum increase of about 15-fold in fluorescence intensity at 635 and 685 nm (Figure 4C). For different tissue grades of dysplasia a similar increasing trend was observed at these wavelengths (Figure 4B). Further, the increase in intensity between different tissue grades is more prominent at 635 nm than that at 685 nm. Nevertheless, the intensity variations at both 635 and 685 nm can be used to distinguish inter- and intra-grades of tissue types. The limited activity of ferrochelatase in heme pathway of malignant tissues hinders the conversion of PpIX to heme, which in turn accelerates accumulation of PpIX and its precursor coproporphyrin III in these lesions.^{24,25}

Corrected LIAF Intensity Ratio. Absorption dips noticed at 545 and 575 nm in the LIAF spectra of tissues are known to be attributed to the presence of HbO₂ in the cells.^{23,36,37} Recently, we reported that HbO₂ absorption of in vivo tis-

ues is greater in the dorsal tongue, buccal mucosa, alveolus, and gingiva compared with that in other anatomic sites of oral cavity.²⁴ Therefore, these absorption anomalies in the autofluorescence spectrum can affect the classification process, especially at locations where hemoglobin absorption is extensive. As reported earlier,³⁷ we have noticed (see Figure 2) that use of diffuse reflectance features in the classification algorithm reduces the influence of variations in blood content and keratinization, and confirms the need to correct the LIAF spectra before computation of the ratios.

Zheng et al¹⁷ used red-to-blue fluorescence image intensity ratios (Ir/Ib) to discriminate malignant oral mucosa from normal. They reported that the mean Ir/Ib of dysplastic tissue (1.1 ± 0.28) is 43.6% higher than the mean value of normal (0.62 ± 0.09). Similar studies were carried out by Zaak et al³⁸ to discriminate malignant bladder tissues from benign with lower false-positive rates. Scott et al¹⁶ proposed the use of red-to-green fluorescence imaging ratios (Ir/Ig) for diagnosis with blue light excitation and found good contrast enhancement between control and malignant samples. After a 4-hour application of 5-aminolevulinic acid (ALA), they observed that Ir/Ig values of normal and dysplastic tissues show a variation of 71%. In comparison, we have noticed that even without the use of any photosensitizer, the raw LIAF ratios F500/F635 and F500/685 were found to be valuable in tissue classification. We also observed a decreasing trend in these ratios with increasing grades of malignancy (Table 2).

Curve-fitted Parameters and Ratios in Tissue Grading. Curve-fitting of the corrected autofluorescence emission from the oral mucosa of healthy volunteers showed 2 peaks at 500.7 and 549 nm, whereas different grades of dysplastic, well-differentiated SCC, and moderately differentiated SCC lesions showed the presence of 4 emission peaks. In poorly differentiated SCC lesions, an additional prominent peak at 705 nm was observed along with the other 4 peaks observed in the lower grades of cancer. During tissue progression from normal to poorly differentiated SCC, the 500.7-nm peak undergoes a red-shift of 10 nm; nevertheless, a larger shift of 72 nm was observed for the 549-nm peak. The corresponding shifts observed in severe dysplastic lesions were 7 and 39 nm, respectively. The Gaussian curve area of the observed peaks was

also found to vary substantially with increasing grades of malignancy. For example, the Gaussian curve area of the 500.7-nm peak decreased significantly by 81% and the area of 635- and 685-nm peaks increased by 120% and 58%, respectively, during transformation from well-differentiated SCC to poorly differentiated SCC. Conversely, the corresponding variations between contiguous lesions such as severe dysplasia and well-differentiated SCC grades were 16%, 19%, and 25%, respectively. The variation in the Gaussian amplitude of the 500.7-nm peak during tissue transformation from normal to poorly differentiated SCC was 98%. The Gaussian peak amplitude and curve area ratios, F500/F635 and F500/F685, follow a decreasing trend with tissue abnormality and show improved detection and grading accuracy than those of corrected LIAF ratios (Table 2). The fluorescence ratios (F500/F635 and F500/F685) based on the Gaussian peak amplitude and

Gaussian curve area of the prominent bands showed improved sensitivities in the intra grading of SCC and dysplasia compared with those of corrected raw spectral ratios.

Detection and Intra-Grading of Premalignancy. Clinically, leukoplakias are considered to be low-risk lesions, which are generally identified histopathologically as hyperplasias, with or without mild to moderate premalignant dysplasia. In most cases, clinical examinations have the potential to identify lesions as normal or abnormal, but fail to classify them as hyperplasia, dysplasia, or SCC. On the contrary, the majority of contemporary optical studies were undertaken to distinguish normal (a group of healthy and benign) from abnormal (a group of dysplastic and malignant) tissues^{22,36,39,40}; or dysplastic from malignant lesions^{21,22,36}; or normal from malignant lesions^{22,41,42}; or cancerous and high-grade dysplasia from low-grade, benign, and

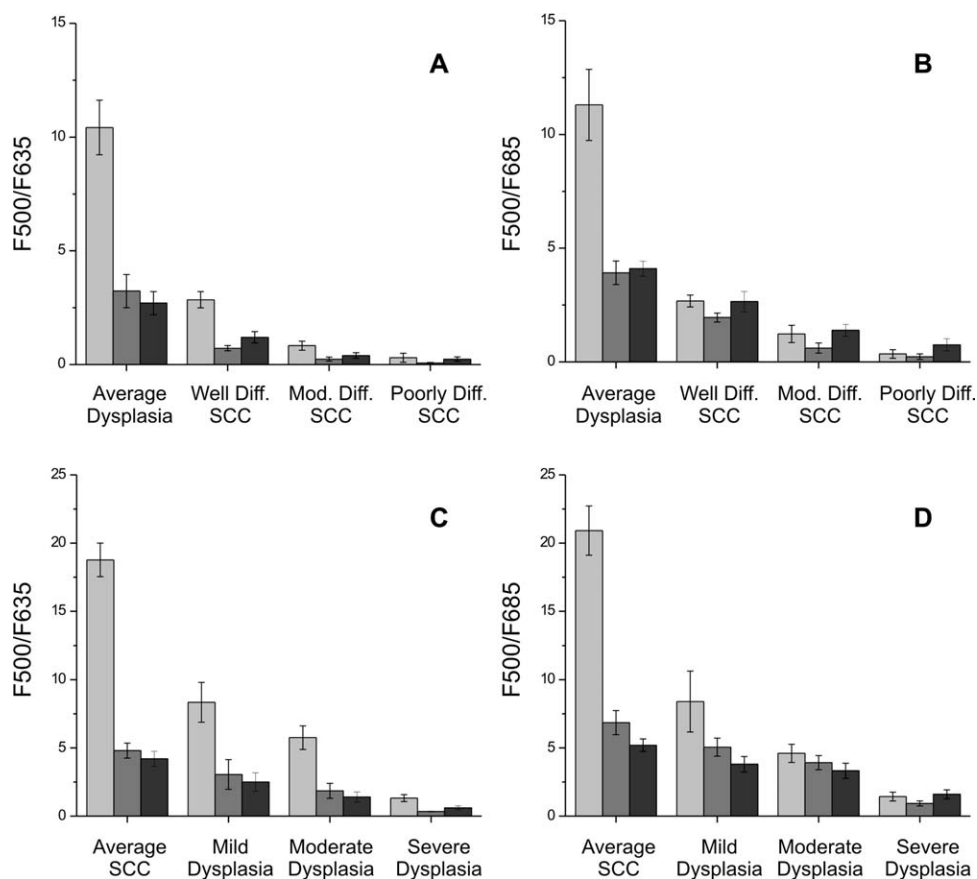


FIGURE 6. Relative decrease in raw spectral and Gaussian area and amplitude ratios with respect to the increase in abnormality of tissues: (A) F500/F635 for intra grades of SCC and average dysplasia; (B) F500/F685 for intra grades of SCC and average dysplasia; (C) F500/F635 for intra grades of dysplasia and average SCC; and (D) F500/F685 for intra grades of SCC and average SCC, with their SDs. SCC, squamous cell carcinoma.

normal.⁴³ The real challenge for any diagnostic system is to detect early tissue transformations—ie, the ability to discriminate premalignant lesions from clinically similar hyperplasias. As a consequence, the relevant question should not be whether the suspicious tissue or lesion is normal or abnormal, but should instead be whether the visible tissue alterations are of a benign or premalignant nature because it has already been established as abnormal from its appearance by the clinician. The answer to this is crucial for classification of incipient lesions and in treatment planning. In this context, the application of curve-fitting on the mean corrected spectra of 17 dysplastic and 8 hyperplastic/hyperkeratotic lesions has shown interesting results.

As can be seen in Table 1, hyperplastic tissues have 2 peaks at 501 and 549 nm, whereas contiguous mild dysplasia to hyperplastic/hyperkeratotic lesions have 4 peaks centered at 506.6, 586.0, 633.5, and 680.7 nm. During tissue transformation from hyperplasia to mild dysplasia, the amplitude and area of the 501-nm peak decrease substantially by 73% and 21%, respectively. Corresponding decreases in the amplitude and area of this peak in mild dysplasias with respect to normal healthy mucosa are 83% and

52%, respectively. Also, a peak shift of about 6 nm is noticed in the 501-nm peak for mild dysplasia with respect to the hyperplasia spectra. The curve-fitted area ratio, F500/F635, for well-differentiated SCC lesions is 45% lower than that of severe dysplastic lesions, whereas the amplitude ratio is 61% higher and the corresponding values for F500/F685 ratio are 41% and 50% higher, respectively (Table 2). Figures 6A to 6D represent variations of F500/F635 and F500/F685 amplitude and area ratios, with their standard deviations, for the different intra-grades of SCC and dysplasia studied.

Sensitivity and Specificity. In this study we have used discrimination scatterplots of the Gaussian amplitude and area ratios (F500/F635 and F500/F685) for grading intra-classes of SCC and dysplasia by correlation with histopathology results. Figures 7A to 7D show the scatterplots of the Gaussian amplitude and area ratios, F500/F635 and F500/F685, belonging to 15 sites in 8 patients, that discriminate lesions categorized as well-differentiated SCC, moderately differentiated SCC, and poorly differentiated SCC. Discrimination lines were drawn between well-differentiated SCC and moderately differentiated SCC, and between moderately

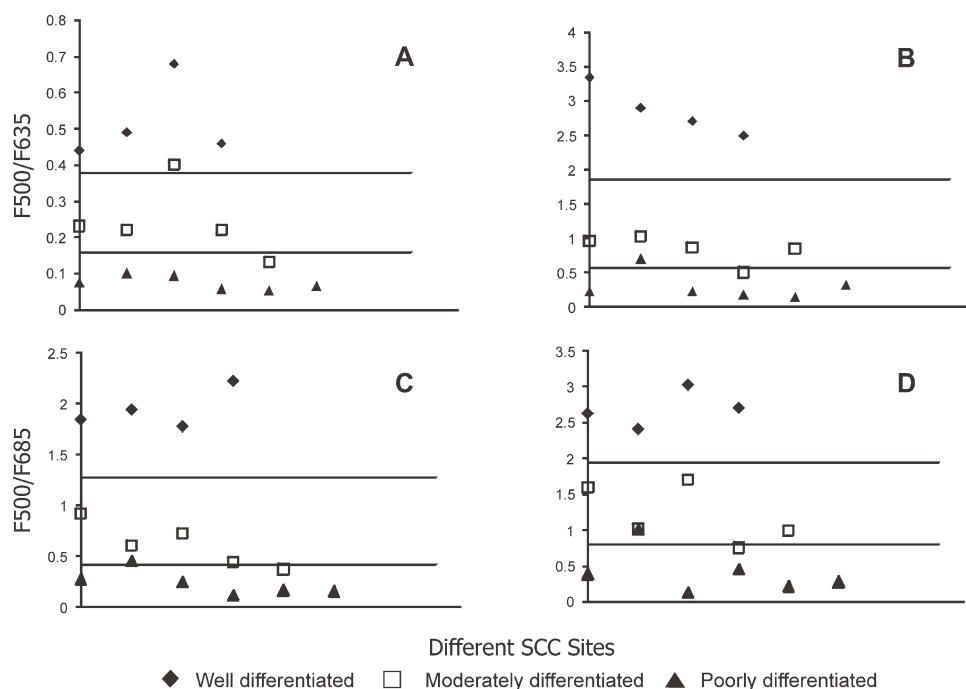


FIGURE 7. Discrimination scatterplots for intra grade lesions of malignant SCC: (A) F500/F635 Gaussian amplitude ratio; (B) F500/F635 Gaussian area ratio; (C) F500/F685 Gaussian amplitude ratio; and (D) F500/F685 Gaussian area ratio, in a study population of 15 lesions. SCC, squamous cell carcinoma.

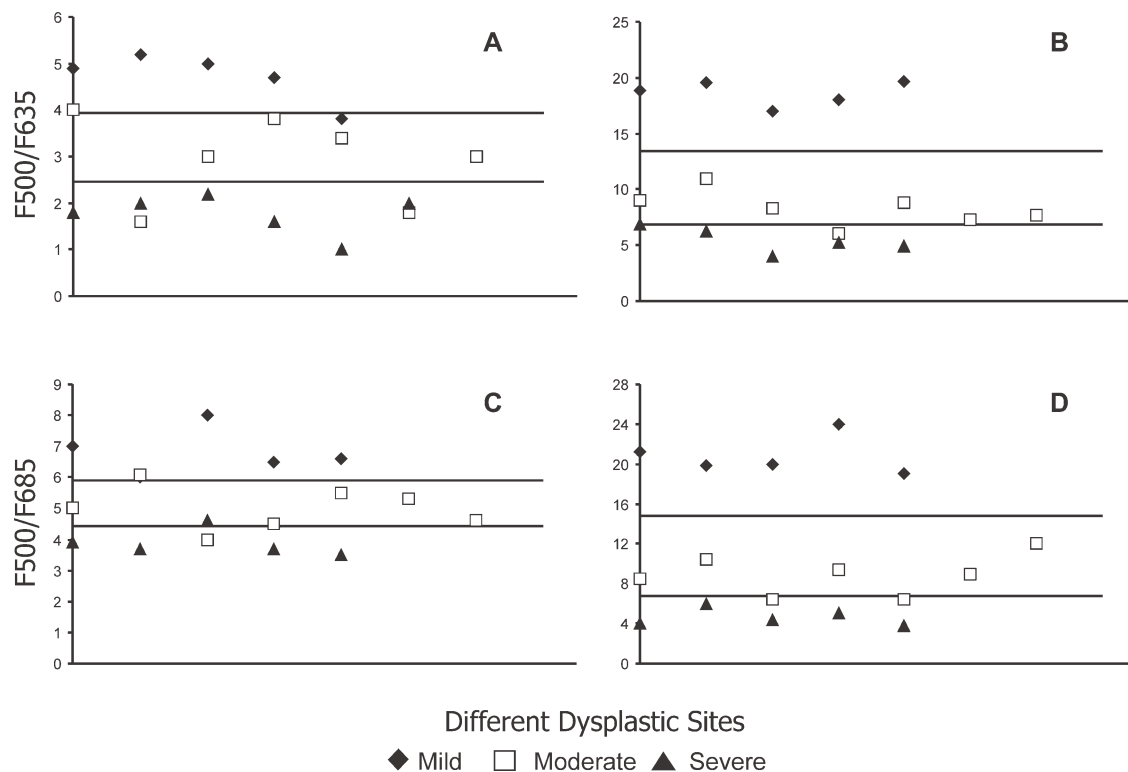


FIGURE 8. Discrimination scatterplots for intra grade lesions of premalignant dysplasia: (A) F500/F635 Gaussian amplitude ratio; (B) F500/F635 Gaussian area ratio; (C) F500/F685 Gaussian amplitude ratio; and (D) F500/F685 Gaussian area ratio, in a study population of 17 lesions.

differentiated SCC and poorly differentiated SCC at values that correspond to the average ratio values of the 2 groups.²⁵ For example, in the case of well-differentiated SCC, the average amplitude ratio values F500/F635 and F500/F685 were 0.62 and 1.52, respectively. The cut-off lines for discriminating well-differentiated SCC from moderately differentiated SCC were drawn at values that correspond to the mean of

well-differentiated SCC ratios and moderately differentiated SCC ratios (0.29 and 0.71, respectively) in patients.

Similarly, Figures 8A to 8D show the discrimination scatterplots of the Gaussian amplitude and area ratios (F500/F635 and F500/F685) from 17 sites in 7 patients, categorized as mild, moderate, and severe dysplasia. The diagnostic accuracies (classification sensitivity and

Table 3. Relative diagnostic accuracies of LIAF Gaussian curve area ratios, F500/F635 and F500/F685, in discriminating different tissue types in vivo.

Gaussian parameters	Relative diagnostic Accuracies	Gaussian LIAF ratios	Mild (5) vs moderate (7) dysplasia	Moderate (7) vs severe (5) dysplasia	Severe dysplasia (5) vs WDSCC (4)	WDSCC (4) vs MDSCC (5)	MDSCC (5) vs PDSCC (6)
Area	Sensitivity, %	F500/F635	100	80	100	100	83
		F500/F685	100	100	100	100	83
	Specificity, %	F500/F635	100	86	100	100	80
		F500/F685	100	71	80	100	80
Amplitude	Sensitivity, %	F500/F635	80	100	100	80	100
		F500/F685	86	80	100	100	83
	Specificity, %	F500/F635	80	71	100	100	80
		F500/F685	100	86	100	100	80

Abbreviations: LIAFS, laser-induced autofluorescence; WDSCC, well-differentiated squamous cell carcinoma; MDSCC, moderately differentiated squamous cell carcinoma; PDSCC, poorly differentiated squamous cell carcinoma.
Note: Values in parentheses show number of sites studied.

specificity) in discriminating each of these categories were determined based on the discrimination threshold values, by validation with the gold standard (ie, histopathologic results of biopsies from the measurement sites).

Table 3 illustrates the relative sensitivity and specificity based on the diagnostic scatterplots. The analysis produced the same specificity and sensitivity of 100%, for both the F500/F635 and F500/F685 amplitude ratios, to discriminate premalignant severe dysplasia from contiguous well-differentiated SCC, whereas both the F500/F635 and F500/F685 area ratios showed a sensitivity of 100% with specificities of 100% and 80%, respectively. The unpaired Student's *t* test value of $p < .005$ for all categories revealed the level of accuracy and statistical reliability of the classification technique. In comparison, Wang et al⁴⁴ reported a sensitivity of 81% and a specificity of 96% using partial least-squares and artificial neural network, whereas Heintzelman et al¹² obtained a sensitivity of 90% and a specificity of 100% for distinguishing abnormal tissues consisting of premalignant and malignant lesions from normal (healthy) and benign mucosa. Further, Muller et al²² achieved an overall sensitivity and specificity of 96%, by using a combination of tissue autofluorescence, diffuse reflectance, and scattering measurements in distinguishing abnormal (cancerous and dysplastic) from normal tissues. However, they were able to classify dysplastic tissues from cancerous with a sensitivity of 64% and specificity of 100%. Fur-

ther, by using these discrimination scatterplots it was possible to discriminate between intra-SCC lesions; moreover, we observed that the differentiation between well-differentiated SCC and moderately differentiated SCC was more accurate, compared with moderately differentiated SCC and poorly differentiated SCC lesions.

Detection of dysplasia is a critical element in improving survival rates and determining therapy, although it is extremely challenging. Many novel optical techniques have been developed to address this problem. Some of these modalities show great promise as stand-alone techniques, although only few have solved this pivotal challenge to the point of clinical adoption with the ability to discriminate hyperplasia (benign) from dysplasia with sufficient sensitivity and specificity. Because porphyrin peaks are associated only with abnormal dysplastic and SCC lesions, to differentiate between normal and hyperplasia, and hyperplasia and mild dysplasia, we have used discriminating scatterplots of curve-fitted area and amplitude of the 501- and 549-nm peaks (Table 1). These scatterplots together have produced an overall sensitivity of 100% and specificity of 86% to discriminate premalignant (mild dysplasia) from hyperplasia/hyperkeratotic tissues, whereas corresponding values in discriminating normal from hyperplasia/hyperkeratotic are 89% and 100%, respectively. It could also be possible to use the Gaussian parameters of the 501- and 549-nm peaks in grading tissues of dorsal tongue, lateral tongue, and

Table 4. Comparison of the diagnostic accuracies of the present study with LIAFS and ESS/DRS spectral criteria of different international groups to distinguish in vivo hyperplasia (benign) from premalignant dysplasia.

Research group	Methodology	Study site, population	Sensitivity, %	Specificity, %
Lovat et al ⁴⁵	ESS, classification by leave 1 out and block validation statistical approach	Esophagus, 181 lesions	79	79
Anjan Dhar et al ⁴¹	ESS, statistically validated model using PCA and LDA	Colon, 138 lesions	85	88
de Veld et al ²¹	LIAFS and DRS, PCA with various classifiers	Oral, 115 lesions	77	76
Nordstrom et al ⁴⁶	DRS and UV-excited fluorescence, multivariate algorithm	Cervical, 120 lesions	77	76
Ge et al ⁴⁷	DRS, pattern-recognition algorithms, including MLR and LDA	Colon, 76 lesions	85	81
Ge et al ⁴⁷	DRS, pattern-recognition algorithms, including BNN	Colon, 76 lesions	82	82
Nieman et al ⁴⁸	OPRS, LDA	Oral, 57 lesions	96	77
Jayanthi et al ⁴⁹	LIAFS, statistically validated model using PCA and LDA	Oral, 34 lesions	78	100
Mallia et al ²⁵	LIAFS, SRRS using scatterplots	Oral, 61 lesions	100	96
Mallia et al ²⁴	DRS, HbO ₂ absorption intensity ratios	Oral, 49 lesions	100	86
Present study*	Curve-fitting Gaussian area and amplitude ratios of corrected LIAF spectra using DR spectra	Oral, 40 lesions	100	86

Abbreviations: LIAFS, laser-induced autofluorescence spectroscopy; ESS, elastic scattering spectroscopy; DRS, diffuse reflectance spectroscopy; PCA, principal component analysis; LDA, linear discriminant analysis; UV, ultraviolet; MLR, multiple linear regression; BNN, back-propagating neural network; OPRS, oblique polarized reflectance spectroscopy; SRRS, spectral ratio reference standard.

*Includes intragrating of dysplastic and squamous cell carcinoma lesions.

vermilion border of lip that show porphyrin-like peaks in healthy tissues attributed to the bacterial colonization.^{20,25} We have observed that the presence of these abnormal peaks in healthy tissues leads to erroneous diagnostic results and affects the diagnostic accuracies.²⁵ Table 4 gives a comparison of the diagnostic accuracies of fluorescence and diffuse reflectance measurements with the results obtained by other research groups for *in vivo* discrimination of hyperplasia from dysplasia. Identifying dysplastic lesions from hyperplasia was 1 of the main aspects of this study; however, alongside the issue of identifying potentially progressive lesions within the dysplastic lesions—especially the early grades of malignancy—was also attempted.

An imperative drawback of histopathology is that the biopsy results are not always representative of the complete lesion. An oral lesion can contain local premalignant changes at 1 position, whereas it can still be benign/malignant at a position only a few millimeters away. This often results in underdiagnosis and usually leads to the numerous random biopsies if the oral oncologist is not convinced that a lesion is benign. These multiple biopsies can result in severe discomfort for the patient. Further, multiple-stage sample preparation and analysis are time-consuming and increase pathologic costs. In comparison, the LIAF technique can quickly survey multiple tissue sites and categorize tissues as normal, benign, premalignant, or malignant before the tissue removal for biopsy. Not only can this optimize sampling from tissue sites that are most likely to be abnormal or premalignant or malignant, but it can also minimize unnecessary removal of normal tissues, thus making the biopsy procedure more accurate and less traumatic to the patient, while also reducing the number of biopsies that need to be processed to obtain a confirmatory diagnosis. Both the lateral spread of malignancy and early tissue transformations could now be noninvasively assessed by inserting the Gaussian amplitude and area ratios calculated from questionable tissue spectra in the corresponding discrimination scatterplots (derived from a larger patient population) for tissue grading in almost real time.

CONCLUSIONS

Results of this study elucidate the potential of using corrected autofluorescence spectra alongside curve-fitting to track tissue progression to-

ward malignancy and grade them accordingly into major groups—ie, normal, hyperplastic/hyperkeratotic benign, premalignant dysplasia, and malignant SCCs. Based on our findings, we report that tissue alterations not only affect the fluorescence spectral intensities, but also alter the spectral shape, as evidenced by the appearance of new peaks, peak shifts, and variations in curve-fitted peak area, intensity, and bandwidth. Further, by use of curve-fitting with Gaussian spectral functions, we were able to locate the exact peak position, area under each peak, and amplitude of the constituent peaks in the LIAF spectra recorded from different types of oral mucosa under *in vivo* environments, and to use these parameters to distinguish different grades of oral cancer/precancer. The curve-fitted Gaussian area and amplitude ratios, F500/F635 and F500/F685, were sensitive to tissue alterations, and the changes in these fluorescence intensity ratios were much more robust and distinct than were raw spectral intensity ratios. Among the 2 spectral ratios, the Gaussian curve area ratio (F500/F635) showed higher diagnostic accuracy.

A notable distinction between premalignant severe dysplastic lesions and well-differentiated SCC was achieved in our clinical trials, with a relative sensitivity and specificity of 100%, by tracking changes in the curve-fitted F500/F635 area and amplitude ratio. The important clinical challenge of distinguishing the hyperplastic/hyperkeratotic lesions from mild dysplastic lesions was achieved with a sensitivity of 100% and specificity of 86%. Our studies have shown that the LIAF technique is an alternative modality for early diagnosis of cancer, and has the potential for use in tissue grading. Eventually, a subset of hyperkeratosis and hyperplasia (leukoplakia) without dysplasia may progress to cancer. It is this subset that should be subjected to intense analysis using tissue autofluorescence. Toward this, a temporal follow-up study in the same patient cohort with a 6- to 12-month perspective is required.

The study has shown that tissue autofluorescence can provide premalignant/malignant tissue grading and also act as an adjunct to the visual examiners, to locate the most malignant portion of the lesion under question. This helps to eliminate the subjective nature of the histopathology and to identify lesion margins for surgeons. Nonetheless, the modality could bridge the gap between clinical examination and

histopathology; furthermore, because it is noninvasive in nature, this technique has the potential for mass screening of random populations through community centers, in particular as a screening tool in a rural nonspecialized setting that allows follow-up studies for identifying high-risk oral lesions and precancer. Although the discrimination criteria were developed for oral cancer diagnosis, these could be extended for diagnoses of different grades of cervical intraepithelial neoplasia (CIN I–III), carcinoma of cervix, and other types of superficial skin cancers. This modality can also be adapted to act as an adjunct to various visual examinations, such as VIA (visual inspection with acetic acid), VILI (visual inspection with Lugol's iodine), colposcopic examination of cervix, and endoscopic examination of the gastrointestinal tract, colon, and stomach.

Acknowledgments. The authors thank the Research Council (RC) of the Centre for Earth Science Studies (CESS) and the Institutional Review Board and Ethics Committee of the Regional Cancer Centre (RCC) for their approval, encouragement, and support. RJM acknowledges the Department of Science and Technology (DST) and Council of Scientific and Industrial Research (CSIR), New Delhi. We are grateful to all the healthy volunteers and patients for their willingness to take part in the clinical trials and also to the postgraduate students who have assisted us in this study. Spectral measurements were carried out at the outpatient clinic of the RCC, Trivandrum, India. Prior approval of the protocol was obtained from the Ethics Committee of the RCC for conduct of clinical trials. After explaining the modalities of the study, written informed consent was obtained from each patient/volunteer prior to enrollment.

REFERENCES

- Boing CC, Squires TS, Tong T, Montgomery S. Cancer statistics. *CA Cancer J Clin* 1994;44:7–26.
- Shafer WG, Waldron CA. Erythroplakia of the oral cavity. *Cancer* 1975;36:1021–1028.
- Drezek R, Sokolov K, Utzinger U, et al. Understanding the contributions of NADH and collagen to cervical tissue fluorescence spectra modelling, measurements, and implications. *J Biomed Opt* 2001;6:385–396.
- Richards-Kortum R, Sevick-Muraca E. Quantitative optical spectroscopy for tissue diagnosis. *Annu Rev Phys Chem* 1996;47:555–606.
- de Veld DCG, Witjes MJH, Sterenberg HJCM, Roodenburg JLN. The status of in vivo autofluorescence and imaging for oral oncology. *Oral Oncol* 2005;41:117–131.
- Lin WC, Toms SA, Johnson M, et al. In vivo brain tumor demarcation using optical spectroscopy. *Photochem Photobiol* 2001;73:396–402.
- Wu T, Qu JY, Cheung TH, et al. Preliminary study of detecting neoplastic growths in vivo with real time calibrated autofluorescence imaging. *Optic Exp* 2003;11:291–298.
- Wagnieres GA, Star WM, Wilson BC. In vivo fluorescence spectroscopy and imaging for oncological applications. *Photochem Photobiol* 1998;68:603–632.
- Schantz SP, Kolli V, Savage HE, et al. In vivo native cellular fluorescence and histological characteristics of head and neck cancer. *Clin Cancer Res* 1998;4:1177–1182.
- Eker C, Rydell R, Svanberg K, Anderson-Engels S. Multivariate analysis of laryngeal fluorescence spectra recorded in vivo. *Lasers Surg Med* 2001;28:259–266.
- Ingrams DR, Dingra JK, Roy K, et al. Autofluorescence characteristics of oral mucosa. *Head Neck* 1997;19:27–32.
- Heintzelman DL, Utzinger U, Fuchs H, et al. Optimal excitation wavelengths for in vivo detection of oral neoplasia using fluorescence spectroscopy. *Photochem Photobiol* 2000;72:103–113.
- Gillenwater A, Jacob R, Ganeshappa R, et al. Noninvasive diagnosis of oral neoplasia based on fluorescence spectroscopy and native tissue autofluorescence. *Arch Otolaryngol Head Neck Surg* 1998;124:1251–1258.
- Savage H, Kolli V, Ansley J, et al. Innate tissue fluorescence of the oral mucosa of controls and head and neck cancer patients. In: Alfano RR, editor. *Proceedings of advances in lasers and light spectroscopy to diagnose cancer and other diseases II*. Bellingham, WA: SPIE, 1995; 2387. pp 2–14.
- Roy K, Bottril I, Ingrams DR, et al. Diagnostic fluorescence spectroscopy of oral mucosa. In: Anderson R, editor. *Proceedings in lasers in surgery: advance characterization, therapeutics and systems V*. Bellingham, WA: SPIE, 1995; 2395. pp 135–142.
- Scott MA, Hopper C, Sahota A, et al. Fluorescence photodiagnosics and photobleaching studies of cancerous lesions using ratio imaging and spectroscopic techniques. *Lasers Med Sci* 2000;15:63–72.
- Zheng A, Soo KC, Sivanadan R, Olivo M. Detection of neoplasms in the oral cavity by digitized endoscopic imaging of 5-aminolevulinic acid-induced protoporphyrin IX fluorescence. *Int J Oncol* 2002;21:763–768.
- Svistun E, Alizadeh-Naderi R, El-Naggar A, et al. Visual enhancement system for detection of oral cavity neoplasia based on autofluorescence. *Head Neck* 2004;26:205–215.
- Lane PM, Gilhuly T, Whitehead P, et al. Simple device for the direct visualization of oral-cavity tissue fluorescence. *J Biomed Opt* 2006;11:024006.
- de Veld DC, Skurichina M, Witjes MJH, et al. Autofluorescence characteristics of healthy oral mucosa at different anatomical sites. *Laser Surg Med* 2003;23:367–376.
- de Veld DC, Marina S, Max JHW, et al. Autofluorescence and diffuse reflectance spectroscopy for oral oncology. *Laser Surg Med* 2005;36:356–364.
- Muller MG, Valdez TA, Georgakoudi I, et al. Spectroscopic detection and evaluation of morphologic and biochemical changes in early human oral carcinoma. *Cancer* 2003;97:1681–1692.
- Subhash N, Mallia RJ, Thomas SS, et al. Oral cancer detection using diffuse reflectance spectral ratio R540/R575 of oxygenated hemoglobin bands. *J Biomed Opt* 2006;11:014018.
- Mallia RJ, Thomas SS, Mathews A, et al. Oxygenated hemoglobin diffuse reflectance ratio for in vivo detection of oral pre-cancer. *J Biomed Opt* 2008;13:041306.
- Mallia RJ, Thomas SS, Mathews A, et al. Laser-induced autofluorescence spectral ratio reference standard for early detection of oral cancer. *Cancer* 2008;112: 1503–1512.

26. Diamond KR, Farrell TJ, Patterson MS. Measurement of fluorophores concentrations and fluorescence quantum yield in tissue-simulating phantoms using three diffusion models of steady state spatially resolved fluorescence. *Phys Med Biol* 2003;48:4135–4149.
27. Muller MG, Georgakoudi I, Zhang Q, Feld MS. Intrinsic fluorescence spectroscopy in turbid media: disentangling effects of scattering and absorption. *Appl Opt-OT* 2001;40:4633–4646.
28. Subhash N, Mazzinghi P, Agati G, Fusi F, Lercari B. Analysis of laser-induced fluorescence line shape of intact leaves; application to UV stress detection. *Photochem Photobiol* 1995;62:711–718.
29. Kollias N, Zonios G, Stamatas G. Fluorescence spectroscopy of skin. *Vib Spectrosc* 2002;28:17–23.
30. Ramanujam N. Fluorescence spectroscopy in vivo. In: Meyers R, editor. *Encyclopedia of analytical chemistry*. Chichester, UK: John Wiley & Sons Ltd, Biomedical Spectroscopy Section, 2000; Vol. 1. pp 20–56.
31. DaCosta RS, Anderson H, Wilson B. Molecular fluorescence excitation-emission matrices relevant to tissue spectroscopy. *Photochem Photobiol* 2003;78:384–392.
32. Huang Z, Zheng W, Xie S, et al. Laser-induced autofluorescence microscopy of normal and tumor human colonic tissue. *Int J Oncol* 2004;24:59–63.
33. Li B, Xie S. Autofluorescence excitation-emission matrices for diagnosis of colonic cancer. *World J Gastroenterol* 2005;11:3931–3934.
34. de Veld DC, Marina S, Max JHW, et al. Clinical study for classification of benign, dysplastic, and malignant oral lesions using autofluorescence spectroscopy. *J Biomed Opt* 2004;9:940–949.
35. Moesta KT, Ebert B, Handke T, et al. Protoporphyrin IX naturally occurs in colorectal cancers and their metastases. *Cancer Res* 2001;61:991–999.
36. Mourant JR, Bigio IJ, Boyer J, et al. Elastic scattering spectroscopy as a diagnostic tool for differentiating pathologies in the gastrointestinal tract; preliminary testing. *Lasers Surg Med* 1995;17:350–357.
37. Zonios G, Perelmann LT, Backmann V, et al. Diffuse reflectance spectroscopy of human adenomatous colon polyps in vivo. *Appl Optics* 1999;38:6628–6637.
38. Zaak D, Frimberger D, Steep H, et al. Quantification of 5-aminolevulinic acid induced fluorescence improves the specificity of bladder cancer detection. *J Urol* 2001;166:1665–1669.
39. Volynskaya Z, Haka AS, Bechtel KL, et al. Diagnosing breast cancer using diffuse reflectance spectroscopy and intrinsic fluorescence spectroscopy. *J Biomed Opt* 2008;13:024012.
40. Zhu C, Palmer GM, Breslin TM, Harter J, Ramanujam N. Diagnosis of breast cancer using diffuse reflectance spectroscopy: comparison of a Monte Carlo versus partial least squares analysis based feature extraction technique. *Lasers Surg Med* 2006;38:714–724.
41. Anjan Dhar DM, Johnson KS, Novelli MR, et al. Elastic scattering spectroscopy for the diagnosis of colonic lesions: initial results of a novel optical biopsy technique. *Gastrointest Endosc* 2006;63:257–261.
42. Bigio IJ, Bown SG, Briggs G, et al. Diagnosis of breast cancer using elastic-scattering spectroscopy; preliminary clinical trials. *J Biomed Opt* 2000;5:221–228.
43. Park SY, Follen M, Milbourne A, et al. Automated image analysis of digital colposcopy for the detection of cervical neoplasia. *J Biomed Opt* 2008;13:014029.
44. Wang CY, Chiang HK, Chen CT, et al. Diagnosis of oral cancer by light induced autofluorescence spectroscopy using double excitation wavelengths. *Oral Oncol* 1999;35:144–150.
45. Lovat LB, Johnson K, Mackenzie GD, et al. Elastic scattering spectroscopy accurately detects high grade dysplasia and cancer in Barrett's oesophagus. *Gut* 2006;55:1078–1083.
46. Nordstorm RJ, Burke L, Niloff JM, Myrtle JF. Identification of cervical intraepithelial neoplasia (CIN) using UV-excited fluorescence and diffuse-reflectance tissue spectroscopy. *Lasers Surg Med* 2001;29:118–127.
47. Ge Z, Schomacker KT, Nishioka NS. Identification of colonic dysplasia and neoplasia by diffuse reflectance and pattern recognition technique. *Appl Spectrosc* 1998;52: 833–845.
48. Nieman LT, Kan C-W, Gillenwater A, Markey MK, Sokolov K. Probing local tissue changes in the oral cavity for early detection of cancer using oblique polarized reflectance spectroscopy: a pilot clinical trial. *J Biomed Opt* 2008;13:024011.
49. Jayanthi JL, Mallia RJ, Thomas SS, et al. Discriminant analysis of autofluorescence spectra for classification of oral lesions in vivo. *Lasers Surg Med* 2009;41:345–352.